BlockChain and Deep Learning with Dynamic Pattern Features for Lung Cancer Diagnosis

A. Angel Mary[1], Dr. K.K. Thanammal[2]
Research Scholar, Department of Computer Science and Research Centre, S.T. Hindu College, Nagercoil, 629002, Manonmanium Sundaranar University, Abishekapatti, Tirunelveli, 627012, Tamilnadu, India[1]
Assistant Professor, Department of Computer Science and Research Centre, S.T. Hindu College, Nagercoil[2]

***Abstract*—Cancers in the respiratory tract grow out of control in lung carcinoma, a deadly disease. Because cancers have irregular shapes, it can be challenging to diagnose them and determine their sizes and forms from imaging studies. Furthermore, a serious issue with health image inquiry is large disparity. Artificial intelligence and blockchain are two cutting-edge advances in the healthcare industry. This paper introduces a Blockchain with a deep learning network for the early diagnosis of lung cancer in an effort to address these problems. Images from CT scans and CXRs were included in the LIDC-IDRI and NIH Chest X-ray collection. Initially, these images are pre-processed by Contrast Limited Adaptive Histogram Equalization (CLAHE) to enhance the image clarity and reduce the noise. Then the Honey Badger optimization Algorithm (HBA) is used to segment the lung region from the pre-processed image. Morphological segments of the lung region are used to generate dynamic patterns. Finally, these patterns are aggregated into the deep neural Spiking Convolutional Neural Network (SCNN), which is the global model for classifying the images into normal and abnormal cases. Based on the classification, the SCNN model achieves 98.64% accuracy from the LIDC-IDRI database and 98.9% on the NH Chest X-ray lung image dataset. The experiments indicate that the proposed approach results in lower energy consumption and faster inference times. Furthermore, the interpretability of the classification findings is improved by the intrinsic explainability of SCNNs, offering more profound understanding of the decision-making process. With these benefits, SCNNs are positioned as a reliable and effective technique for classifying lung images, providing a significant advancement over current methods.**

Keywords*—Lung cancer; spiking convolutional neural network; LIDC-IDRI; CLAHE; Honey Badger optimization Algorithm; segmentation; classification

I. INTRODUCTION

As the primary cause of cancer-related fatalities worldwide, lung cancer is also one of the most often diagnosed malignancies. The World Health Organization predicted that in 2020, there would be over 1.8 million lung cancer deaths and about 2.21 million new cases of the disease. In addition, it is estimated that 17 million people worldwide would suffer from cancer by 2030 [1]. Cigarette smoking, the primary cause of lung cancer, accounts for 80% of the disease's mortality. Exposure to radon gas is the second most prevalent cause of lung cancer [2]. Only 21% of cases of early-stage lung cancer are identified at stage I, with most cases being detected at stage III or IV (representing 61% of all newly discovered lung cancers)due to the disease's characteristic lack of symptoms [3]. The high fatality rate and aggressive nature of the illness are mainly due to late-stage detection [4]. In order to lower the death rate from lung cancer, early detection of smaller tumours and nodules using X-rays and CT scans is especially crucial because the prognosis for early treatment is noticeably better than that for later stages.

Due to the complicated anatomy of the lungs, many clinical decisions support systems, particularly machine learning techniques, rely on segmentation. Information technology has advanced recently beyond only making people's lives easier; the outcome is AI technology that offers healthcare facilities and improved quality of life. It is acknowledged that efficient data collection, processing, analysis, and safe storage are essential procedures. The first and most important challenge is the ongoing inflow of data into the medical field; this issue might be crucial to the development of effective and secure medical data storage. For the purpose of early lung disease diagnosis, a Blockchain with a deep learning network is therefore introduced in this study.

This research work aims to construct automated lung cancer detection using region-based segmentation methods with tumor area detection and subsequently to develop an effective system for the classification of lung tumors. In order to minimize the noise present in the CXR images, these pictures undergo pre-processing using Contrast Limited Adaptive Histogram Equalization (CLAHE). Segmenting the lung cancer area is done by Honey Badger optimization Algorithm (HBA). Dynamic patterns are produced using morphological segments of the lung cancer area. Dynamic pixels are created by further separating the segmented pictures into different cells. Finally, a novel deep Spiking Convolutional Neural Network (SCNN) is used to classify normal and abnormal cases by using CT and Chest X-ray images.

In the proposed architecture, trust between local nodes at the global node layer is maintained by a reputation system based on blockchain technology. By segmenting the neural network into several networks, each with a limited set of permitted entities, storing data on the cloud gate server and allowing applications to undertake data analysis, the security of the medical data is guaranteed. Its flexibility and agility in solving intricate non-linear problems is one of its advantages. Its capacity to tackle intricate non-linear problems with great flexibility and adaptability is one of its advantages. When compared to current deep neural networks, our method yields better and more accurate results. It may be applied in medical

facilities to advance AI research and enhance early diagnosis of lung diseases.

The key contributions of the proposed model:

In this work, multi-modal images such as CT and CXR images are used for lung disease classification in early diagnosis.

To detect the lung cancer easily, segmentation process is applied. Honey badger optimization (HBA) is used for lung disease segmentation and the morphological segments of the lung region are used to generate dynamic patterns.

These dynamic patterns and output local nodes are aggregated into the deep neural Spiking Convolutional Neural Network (SCNN), also known as Global network, for classifying the input images into normal and abnormal cases.

To prevent privacy protection and secure the classification results, the block chain technology is designed.

II. Literature Survey

This review offers a general overview of deep learning-based image processing techniques used in both classic and modern methods to diagnose lung cancer.

A unique filtering method that eliminates unnecessary pictures and lowers false-positives has been presented by Liang et al. [5] for the classification of lung nodules. To locate lung nodules precisely, they employed Faster R-CNN. According to the study's findings, this method could successfully identify pulmonary nodules in CT images, which could help doctors identify lung cancer early on.

A novel deep learning model has been suggested by Asuntha et al. [6] to identify lung nodules. To extract features, one can employ feature descriptors such as wavelet transform-based features, Zernike Moment, Scale Invariant Feature Transform (SIFT), Histogram of Oriented Gradients (HoG), Local Binary Pattern (LBP), and so on. The Fuzzy Particle Swarm Optimisation (FPSO) approach is utilised to choose the best feature. Deep learning techniques are employed for classification. To lessen the network's computational complexity, a unique FPSOCNN is employed.

A novel method for classifying lung images has been suggested by Vas et al. [7]. This method uses a median filter during the preprocessing stage to eliminate the unnecessary portion of the image. Accurate lung segmentation and cancer diagnosis are made possible by the application of mathematical morphological techniques. From the divided region, the following data were extracted: energy, correlation, variance, homogeneity, difference entropy, contrast and correlation information measure. These were then sent to the feed forward neural network using the back propagation technique for classification.

An enhanced lung nodule identification method based on the YOLO-V3 target detection network was presented by Li et al. [8]. This article uses the Mask-RCNN network and enhances it using the channel shuffle convolution method and Densenet's dense block structure. A computer-aided technique for the early identification of lung cancer using CT images was proposed by Elnakib et al. [9]. A genetic algorithm (GA) is trained to optimize the obtained data set in order to determine the most significant elements. A variety of classifiers are finally looked at in order to identify the pulmonary nodules properly. Comparing the suggested technology to other earlier methods like VGG-16, AlexNet and VGG-19 networks, encouraging results are obtained.

Srinivasulu et al. [10] introduced a novel blockchain based lung cancer detection using extended CNN. There are primarily two architectures like U-Net and VGG-16 are used in the suggested method to categorize lung nodules and predict the amount of malignancy. The Internet of Things (IoT) may be used for the proposed multistage lung cancer detection and classification,

An algorithm for detecting lung nodules has been developed by Vaishnavi et al. [11]. For pre-processing, they used a discretely sampled wavelet in the Dual-tree complex wavelet transform (DTCWT). GLCM is a texture analysis technique that determines how often different Grey level combinations co-occur in an image using a second-order statistical method. They used a Probability Neural Network (PNN) classifier, whose accuracy in classification and training was evaluated.

The Faster R–CNN method for lung cancer detection was first described by Su et al. [12]. They illustrate the quicker R-CNN's suitability for lung knob recognition based on the training set. CNN and alternative optimization are the two training techniques used in the Faster R–CNN approach. Low tiny object identification accuracy is a common problem with many network models; hence, in order to increase the sensitivity to small things, the model needs to be enhanced and optimized.

A cat swarm optimization-based computer-aided diagnostic model for lung cancer classification (CSO-CADLCC) was reported by Vaiyapuri et al. [13]. The Gabor filtering-based noise reduction approach is the first pre-processing method used by the proposed CHO-CADLCC technology. Additionally, the NASNetLarge model is used to extract features from the pre-processed pictures. The CSO method with the weighted extreme learning machine (WELM) model comes next and is used to classify lung nodules. In order to optimise the WELM model's parameter tuning and get better classification performance, the CSO method is finally applied.

Inception V3, CNN, CNN GD, Resnet-50, VGG-16, and VGG-19 are the six deep learning models that Rajasekar et al. [14] suggested be used to diagnose lung cancer effectively. Based on the histopathological and CT scan pictures, experimental studies were carried out. This approach will be effective in detecting lung cancer and helpful to those in need due to the inherent benefit of the suggested methodology. The I3DR-Net is a single-stage detector that was proposed by Harsono et al. [15] to identify and categorise lung nodules. A feature pyramid network with pre-trained image weight from the inflated 3D ConvNet (I3D) was combined with a multi-scale 3D Thorax CT scans database to build the model.

For the purpose of detecting lung nodules, Schultheiss et al. [16] created the CNN-based RetinaNet architecture. The input

picture is segmented using the U-Net technique. An important part of this work was investigating the possibility that foreign substances may cause inaccurate selections in CNN-based nodule recognition systems. A multicrop CNN was presented by Shen et al. [17] that can automatically extract salient module features by max-pooling procedures performed at different times and cropping different sections from feature maps.

A lung nodule classification method based on a deep residual network is proposed in [22]. In [23], the CT image sub-block preprocessing strategy was used to extract nodule features for enhancement and alleviate the aforementioned problems. The experimental results showed that the effective classification time cost based on the original Faster R-CNN detection method. The research in [24] presented the Non-Local network by adding channel-wise attention capability and apply Curriculum Learning principles for the classification task. Assorted Scale Integrated Alternate Link Model Convolutional Neural Network method is proposed in [25] for Lung Nodule Detection. A new hybrid deep learning framework by combining VGG, data augmentation and spatial transformer network (STN) with CNN is proposed in [26]. Multiscale Rotation-Invariant Convolutional Neural Networks technique is designed to find the lung texture classification results [27]. The article [28] offered hybrid CNN along with the SVM classification method with tuned hyperparameters for Lung Cancer Detection from X-Ray Images. Table I presents the summary of existing work.

TABLE I. SUMMARY OF EXISTING WORK

REFERENCES	NETWORKS	ADVANTAGES	LIMITATIONS
[5]	R-CNN	Eliminates unnecessary pictures and lowers false-positives	Model is not strong because of insufficient samples
[6]	FPSOCNN	Find best feature	Can improve the performance with advance classification methods
[7]	FFNN	Eliminate the unnecessary portion, extract some data	insufficient data sample size
[8]	Mask-RCNN	Segmentation and classification	Need to improve the network performance and the recognition accuracy.
[9]	AlexNet	Improved the contrast of image	Insufficient training data
[10]	U-Net	classify and organize and assess threat level	Limited input and output
[11]	PNN	Classify normal and abnormal	Limited pattern neuron
[12]	R–CNN	Improved detection accuracy than existing	Used too small samples
[13]	NASNet	Preprocessing, feature extraction and classification	Can be used more samples
[14]	CNN	histopathological images are considered for the identification	Can be used advanced optimization technique
[15]	3D ConvNet	texture detection and classification	Can be implemented in real-time
[16]	U-Net and RetinaNet	Find critical positions	Used limited images
[17]	MC-CNN	Initialization approach of characterizes nodule semantic attributes	Can use more samples
[22]	ResNet	Less false positive rate	Long training time
[23]	FR-CNN	reduced the rate of misdiagnosis	Used less samples
[24]	ProCAN model	achieved state-of-the-art performances	Can improve accuracy
[25]	ASIAL CNN	More convolutional pathways	Can improve prediction accuracy
[26]	VDS net	Determine the condition of patients	Need more samples
[27]	MRCNN	Change overlapping adjacent patches	Used only CT samples
[28]	OCNN-SVM	Categorizing lung image	Want to use various data sets

III. PROPOSED METHODOLOGY

The proposed work has three stages: (a) Preprocessing, (b) Segmentation and (c) Classification. Fig. 1 demonstrates the proposed work.

A. Pre-processing using CLAHE

The accuracy of the lung image classification process is enhanced by this pre-processing phase. In this work, input CT and Chest X-ray image enhancement is achieved with Contrast Limited Adaptive Histogram Equalization (CLAHE). When compared to AHE, it processes computationally more quickly since there are no overlapping blocks [18]. The CLAHE technique effectively equalises the image histogram in addition to enhancing contrast [19].

One type of adaptive contrast augmentation method is called CLAHE. Adaptive histogram equalisation, or AHE, can be used to sharpen the borders of each picture region and boost local contrast. Updates to the enhancement computation are made for CLAHE using the maximum contrast enhancement factor and the highest clip level value, respectively. After that, the neighbouring picture areas are blended by bilinear interpolation to eliminate artificially stimulated region borders. Using this approach, medical photos can have better quality and contrast. The histograms for each region are first calculated utilising restrictions for contrast expansion and clipping in

order to maximise picture improvement. After that, the calculated histogram is re-distributed to maintain the height inside the clip limit. For CLAHE grayscale mapping, Cumulative Distribution Functions (CDFs) are computed by Eq. (1), and the histogram equalisation is obtained by estimating the CDF.

$$F_{a,b}(q) = \frac{(Q-1)}{P}\sum_{s=0}^{q} r_{a,b}(s)\,. \quad q = 1,2,\ldots..Q-1 \qquad (1)$$

The pixel units and grayscales for each area are given as P and Q in the above assessment. If the histogram of the (a, b) region is$F_{a,b}(q)$, for $q = 1, 2, \ldots..Q-1$, the CDF estimate, scaled by N-1 for grayscale mapping, is provided.

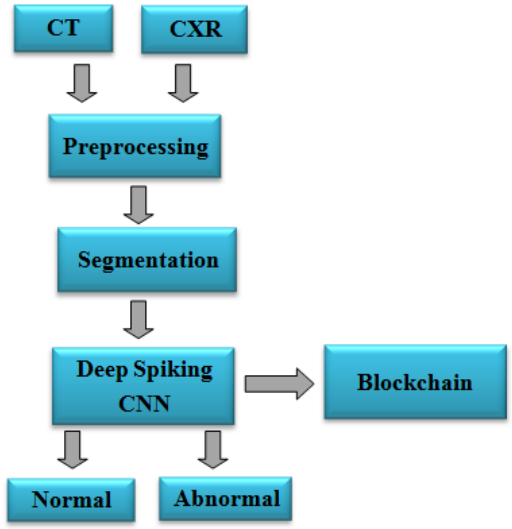

Fig. 1. Schematic representation of lung disease diagnosis framework.

B. Segmentation using Honey Badger Algorithm (HBA)

The Honey Badger Algorithm (HBA) is an excellent segmentation algorithm because of its adaptive balance between exploration and exploitation. This balance enables the algorithm to effectively navigate complex search spaces and avoid local optima. Because of its exceptional boundary detection precision, it can accurately segment images even in difficult cases with overlapping structures or fuzzy edges. It produces consistent results across various datasets and is more adept at managing noise and variability, which are prevalent in medical imaging. Additionally, it is flexible, scalable, and converges quickly, making it suitable for real-time applications.

Hence the HBA is used in the suggested way to benefit from a cutting-edge segmentation method. The segmented images are separated into various cells, which are then further separated into dynamic pixels. The center value and its neighboring bits are selected in each cell in dynamic pattern. Based on the center value, the pattern was generated by changing the gray scale values to binary values. Finding a method that can effectively separate the lungs from the CT and CXR pictures would be great, according to the previous studies. The algorithm's developers called the first technique the "digging phase" and the second the "honey phase". Fig. 2 depicts the honey badger's improved optimization algorithm.

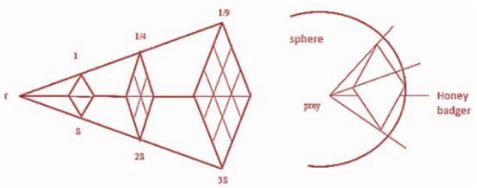

Fig. 2. Basic honey badge algorithm.

This section presents the algebraic formulation of the suggested HBA method. Since HBA includes periods for both exploration and exploitation, a global segmented technique might be considered. The following is a mathematical breakdown of the phases in the proposed HBA.

The following are the main phases of the HBA and the corresponding equations for them: The population of potential solutions for HBA is expressed in Eq. (2).

$$Pops = \begin{bmatrix} x_{11}x_{12}x_{13}\ldots x_{1D} \\ x_{21}x_{22}x_{23}\ldots x_{2D} \\ \ldots \quad \ldots \quad \ldots \quad \ldots \\ x_{n1}x_{n2}x_{n3}\ldots x_{nD} \end{bmatrix} \qquad (2)$$

$x_i = [\,x_i^1,\ x_i^2, \ldots\ldots, x_i^D]$ is the formula for the ith position of the honey badger derived from the previous equations.

1) Step 1 Initialization stage: The issue space's upper (Yu) and lower (Yl) bounds identify the first potential solution at this stage. Consequently, the first solutions, as given by Eq. (3), are made up of random sets that may be generated using the subsequent method.

$$Y_a = Yl + R_1(1,d) \times (Yu - Yl), \qquad a = 1,2,3\ldots..n. \qquad (3)$$

In this case, n solution providers (honey badgers) are given, Y displays every potential solution, and d indicates the magnitude of the solution.

2) Step 2 Updating positions: The Y_{new}coordinates for the candidates have been updated. For example, this may mean excavating or using a strategy that takes advantage of the honey phases. The ability of the hunter's scent and the distance between the prey and the honey badger (F) determine the potential search areas during the digging phase. The honey badger excavates in a circle. The following Eq. (4) describes how it moves:

$$Y_{new} = F + D_i \times \beta \times Min \times F + D_i \times R_3 \times (F - Y_a) \times (cos2\pi R_4) \times (1 - cos2\pi R_5) \qquad (4)$$

where β is the food-gathering capacity of an insect. Using a uniform distribution and a range of 0 to 1, the R_3, R_4, and R_5 are randomly chosen random variables. The level of intensity is attained. As a sign of a search strategy, the D_i is created by the following Eq. (5):

$$D_i = \begin{cases} 1 & if\ R_6 \le 0.5 \\ -1 & if\ else \end{cases} \qquad (5)$$

The honey badger phase Use the honey stage to go over with the lead bird in search of beehives. The honey phase was calculated using the following Eq. (6):

$$Y_{new} = F + D_i \times R_7 \times \sigma \times (F - Y_a) \qquad (6)$$

where R_7 is a randomly generated number between 0 and 1, and F is the highest outcome thus far.

3) Step 3 Modeling intensity min: The following computation in Equation 6 for each candidate's level of odour intensity min of the prey is needed, after which the honey badger's ability to detect insect odour controls its movements.

$$Min = \frac{R_2 \times (Y_a - Y_{a-1})^2}{4\pi(F_p - Y_a)} \quad (7)$$

The prey's location is indicated by F_p in the equation (7) above, and R_2 is an arbitrary sum between 0 and 1.

4) Step 4 Density parameter modeling ($\boldsymbol{\sigma}$): Between the local and global search stages, the information flow is regulated by the sigma value. The following Eq. (8) illustrates the hypothesis that beta is represented throughout every iteration:

$$\sigma = C \times \exp\left(\frac{-r}{r_{max}}\right) \quad (8)$$

Where, the values for r and r_{max}represent the current iteration and the total number of iterations. C stands for constant, and its recommended value is 2.

5) Step 5 Escaping from local results: The search direction is signalled with a warningD_i, which the algorithm authors utilised to avoid becoming stale on regional fixes. HBA is known as a global optimisation method due to its exploration and exploitation stages. HBA is easy to use and understand, and there are fewer operators to alter. Finally, segmented pictures are used to classify lung carcinomas. The segmentation accuracy was measured using the rate of truepositive, rate of true negative, rate of false positive, and rate of falsenegative from the algorithm.

C. Classification using Spiking Convolutional Neural Network (SCNN)

The architecture of a Spiking Convolutional Neural Network (SCNN) is similar to that of traditional Convolutional Neural Networks (CNNs), but it is adapted to work with spike-based representations and to leverage the principles of spiking neural networks (SNNs).

A dynamic pattern refers to how the rules for updating each cell's state vary dependent on multiple circumstances, such as the cell's present state, its neighbours, or external inputs. Each cell has a dynamic pattern of selection for the center value and the bits surrounding it. Binary values were substituted for the grey scale values to create the pattern based on the center value. Ultimately, the global model for categorizing the pictures into normal and abnormal situations is the deep neural Spiking Convolutional Neural Network (SCNN), which is comprised of various patterns. With almost a billion spiking neurons, the Spiking neural network architecture is a massively parallel neurocomputer design intended for categorization. A spike-carrying neural network (SCNN) may broadcast and receive large quantities of information based on the relative timing of its spikes. Basic outline of the SCNN architecture is depicted in Fig. 3:

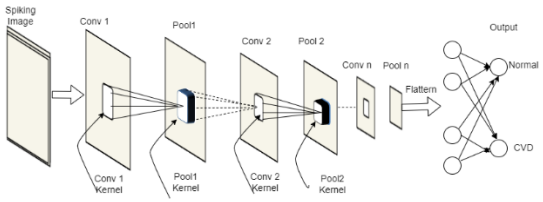

Fig. 3. SCNN network architecture.

As shown in the above figure, the convolutional layer, pooling layer, and spiking fully connected layer comprise the spiking CNN. Both the fully connected layer and the convolutional layer include layer-wise learning.

1) Convolutional layer: The convolutional layer of the network may be constructed after the convolutional filters are obtained. As in a traditional CNN, the convolutional layer employs weight sharing to lower the number of parameters. However, spike trains—rather than actual values—are used to transport the information in a spiking CNN.

The normalized grey scale pixel intensity in the range of (0,1) determines the pace at which spike trains representing the input picture (r × c pixels) are generated. The picture is sent to the network for T = 20 ms split into 1 ms time increments, as was previously mentioned. The convolution process is displayed in the network's first layer, which is illustrated in Fig. 2. To create feature maps with (r − p + 1) × (c − p + 1) LIF neurons, a collection of D filters (trained as mentioned in the previous section) are individually convolved with the picture throughout the 20-time-step presentation period. A particular aspect of the image is represented by each feature map that has LIF neurons in it. When threshold is reached, a LIF neuron in a feature map emits a spike. It aggregates the convolution results for a specific picture patch across T = 20 time steps. Upon firing, the membrane potential is returned to its resting value of zero. The membrane potential, U, of neuron m in feature map k at time t is computed using Eq. (9).

$$\frac{dU_m^k(t)}{dt} + U_m^k(t) = I_m^k(t) \quad (9)$$

If $U_m^k(t) \geq \theta^{conv}$, $then\ U_m^k(t) = 0$

I_m^k is defined below Eq. (10).

$$I_m^k(t) = \sum_{i=1}^{p}\sum_{j=1}^{p} W_k^{ex}(i,j) \,.\, S_m(i,j,t) \quad (10)$$

A representation of the filter's convolution is $I_m^k(t)$. W_k^{ex} , and at T = 20 time steps, the presynaptic spike train, S_m. The spike train that represents a pixel value in the (i,j)coordinate of patch m is called$S_m(i,j)$.

Every neuron receives inputs in the form of $p2$ spike trains with λ_{ij} rate parameters. The predicted value of the injected current at time step t, as determined by filter k for neuron m, is provided by Eq. (11).

$$E[I_m^k(t)] = \sum_{i=1}^{p}\sum_{j=1}^{p} W_k^{ex}(i,j) \,.\, \lambda_{ij} \quad (11)$$

This may be compared to $I = (w^{ex})^T.x$, where w^{ex} is a filter that represents pixel intensities and x is scaled to the average firing rates. Consequently, the convolution over T time steps may be used to approximate classical convolution.

2) Pooling layer: The spike trains generated from the convolutional layers are downsampled by the pooling layers. Spike-based representations allow for the adaptation of max-pooling processes, which usually include choosing the maximum number of spikes inside the pooling areas.

Following convolution, a neuron with the most activity within a square neighborhood of $lp \times lp$ presynaptic neurons is chosen by the pooling layer (max pooling). Additionally, parameter lp acts as the pooling layer's stride value. The spike rate of each neuron in a feature map may be used to describe its activity. Consequently, a feature map measuring $(r - p + 1) \times (c - p + 1)$ is converted to a smaller feature map measuring$(r - p + 1)/lp \times (c - p + 1)/lp$.
Robustness against local translation and scale changes is aided by the max pooling layer. In Fig. 2, the pooling layer appears as the second layer of the network. Nonadaptive relationships exist between the pooling maps and convolutional maps.

3) Fully connected layer: Fully connected layer classifies the image into normal or CVD. The spike trains that are released by the pooling layer divide the image's many visual elements among the D feature maps (D might have values of 16, 32, or 64). The output units receive spike trains emanating from the pooled feature maps at the third layer of the network, known as the fully connected (H) layer. The information's dimension is decreased in the feature maps by this layer.

For a neuron in the H layer to fire at a certain time step, it has to fulfill two requirements. The initial one is that it crosses its conventional LIF threshold, θ^h. Among the other neurons in the H layer, it does well in a non-exclusive winners-take-all (WTA) competition. As a result, we refer to the units in this layer as WTA-threshold LIF neurons. A WTA score is assigned to each unit in the H layer based on how its net input compares to the inputs of the other units in the layer. The synaptic weights,W, and the presynaptic spike vector, y_t, together yield the net input at time t.

$$WTAscore_h(W, y_t) = \frac{e^{W_h^T . y_t}}{\Sigma_{j=1}^{H} e^{W_j^T . y_t}} \quad (12)$$

IV. Secure Management Using Block Chain

Deep learning and blockchain are two extremely innovative technologies that are changing the standard operating procedures in the medical field. Using smart contracts, its solution improves transparency, safety, dependability, and data transmission capabilities. Among blockchain's many notable benefits are the ability to create smart contracts. This enables users to manage data access according to predetermined standards and agreements.

To guarantee that the data is private and secure, the classified lung picture in the proposed work is encrypted. By using encryption, the pictures are protected from being viewed by unauthorized users who do not have the necessary decryption keys to view them on the blockchain. Even if someone acquires unauthorized access to the blockchain, encryption makes sure they are unable to view the image without the correct decryption key.

After that, the encrypted lung image is hashed to provide a distinct digital fingerprint. The process of hashing transforms the image data into a fixed-length string of characters that while uniquely expressing the image, is unretrievable through reverse engineering. This hash serves as the lung image's special identification.

On the blockchain, a block contains the hash of the lung picture and associated metadata. Afterwards, a network of nodes receives this block, which is added to a chain of earlier blocks. Blocks cannot be removed or changed after they are put to the blockchain, making them immutable. By doing this, the classification is permanently preserved and the lung image data is kept impervious to manipulation.

The original image can only be viewed by authorized individuals who possess the relevant decryption key. By automatically providing or refusing access in accordance with pre-established guidelines, smart contracts enforce access policies. Algorithm 1 is the pseudocode for the proposed work.

Algorithm 1: Proposed Work

1: Load Dataset

2: Resize the image

3: Declare CLAHE

4: Threshold for contrast limiting

5: Initialize the number of honeybadger

6: Sort the fitness vale of honeybadger

7: Find optimal value

8: Calculate Density

9: Calculate intensity

10: Find digging phase

11: Sort fitness value

12: Update global optimization solution

13: Train the model

14: Test the model

15: Predict normal or abnormal

16: Integrate Blockchain for Data Integrity

V. Experimental Evaluation

A. Dataset Description

This part implements the LIDC-IDRI dataset to identify instances of lung cancer. The database has 848 nodules that have been enhanced in 17 different methods, 442 of which are benign and 406 of which are malignant. The dataset from LIDC-IDRI contains lesion annotations from four thoracic radiologists with expertise. Included in LIDC-IDRI is 1018 low-dose lung CT scans from 1010 lung patients.

A popular and effective medical imaging technique is a chest X-ray. In certain cases, the clinical examination of CXR pictures might be even more challenging than the study of a

chest CT scan. The 112,120 CX-ray pictures in the NIH Chest X-ray Dataset are associated with individual diseases.

B. Evaluation Metrics

The following statistical measures, including accuracy, precision, F1 score and recall are used to evaluate the efficacy of the proposed lung nodule classification technique. The terms $TruPos$, $TruNeg$, $FalPos$ and $FalNeg$ are represents the True-Positive, True-Negative, False-Positive and False-Negative, respectively. The following equations can be utilized to compute the metrics.

$$Accuracy = \frac{(TruPos + TruNeg)}{(TruPos + FalPos + TruNeg + FalNeg)}$$

$$Precision = \frac{TruPos}{(TruPos + FalPos)}$$

$$Recall = \frac{TruPos}{(TruPos + FalNeg)}$$

$$F1Score = 2 \times \frac{(Recall \times Precision)}{(Recall + Precision}$$

VI. Result

The suggested approach for segmenting and categorizing lung nodules is presented here with the experimental results. The recommended approach was put into practice using a MATLAB environment. Accuracy, F1 score, precision, and recall metrics were used to assess the classification performance. Two sets of lung nodule pictures, such as CT and Chest X-ray (CXR) images, were used for the experiments. Table II shows the classification results of the proposed SCNN model on LIDC-IDRI dataset.

TABLE II. Classification Results of the Proposed SCNN Model on LIDC-IDRI Dataset

Performance Measures	Proposed SCNN
Accuracy	98.64
Precision	92.42
Recall	93.76
F1-score	93.08

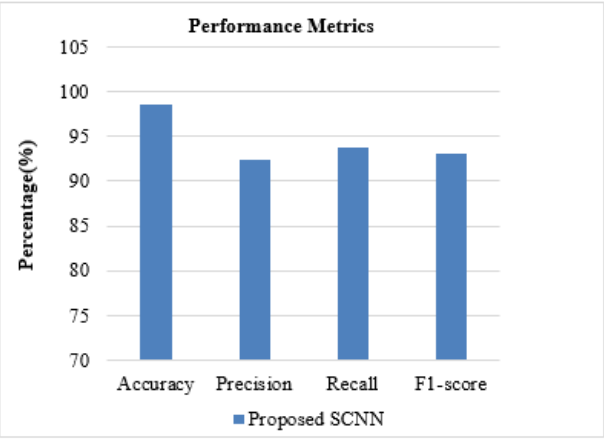

Fig. 4. Performance of the proposed SCNN model on LIDC-IDRI dataset.

The proposed SCNN model achieves 98.64% of accuracy, 92.42% of F1score, 93.76% of precision and 93.08% of recall on LIDC-IDRI images. The effectiveness of the suggested model is visually represented in Fig. 4.

Table III displays the classification results of the proposed SCNN model on NH Chest X-Ray images. The suggested model achieves 98.9% accuracy, 97.3% precision, and 94.44% recall and 95.84% of F1score on NH Chest X-Ray images.

TABLE III. Classification Results of the Proposed SCNN Model on NH Chest X-Ray Dataset

Performance Measures	Proposed SCNN
Accuracy	98.9
Precision	97.3
Recall	94.44
F1-score	95.84

The suggested SCNN classifier's classification performance is illustrated in Fig. 5. It demonstrates that the suggested model produces higher predictions of accuracy, precision, recall, and F1-score across the board. The effectiveness of the suggested model is visually represented in Fig. 5.

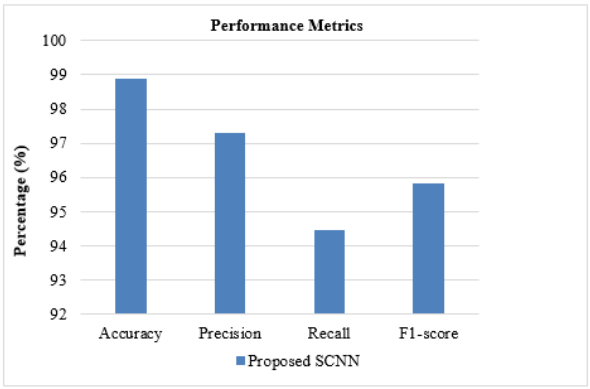

Fig. 5. Performance of the proposed SCNN model on NH Chest X-Ray dataset.

A. Comparative Analysis

A comparison between the suggested model and traditional neural networks is also done in this section. The comparative analysis of Lung cancer detection in terms of accuracy of the proposed Spiking CNN model with existing methods on CT dataset is displayed in Table IV. It is clearly detected that the proposed Spiking CNN classifier gives superior results than the other previous research work based on accuracy. It gives 98.64% of accuracy which is +6.19% than ASAIL CNN approach, +4.53% than ProCAN approach, +8.94% than Improved FasterR-CNN, +2.83% than Inception V3, +0.41% than Deep residual network, +8.74% than ResNet method, +14.5% than CNN model. The results of this technique's performance comparison with standard methods indicate that the proposed method outperforms them.

The intended model yielded better performance than the earlier networks. The expected outcomes seem to be rather reliable in distinguishing between typical and anomalous instances. The result shows the effectiveness of the proposed

model based on blockchain dynamic pattern techniques applied in deep Convolutional Neural Network.

TABLE IV. COMPARATIVE ANALYSIS OF SCNN WITH OTHER CLASSIFIERS ON CT IMAGES

Author/Year	Methods	Accuracy (%)
Song et al./2017 [20]	CNN	84.14
Nibali et al./ 2017 [21]	ResNet	89.90
Wu et al./ 2020 [22]	Deep residual network	98.23
Wu et al/ 2020 [22]	Inception V3	95.81
Shiwei et al. /2021 [23]	Improved FasterR-CNN	89.7
Al-Shabi et al/2022 [24]	ProCAN	94.11
Parveen Banu et al/ 2022[25]	ASAIL CNN	92.45
Proposed Method	SCNN	98.64

Fig. 6 presents a visual representation of the comparison findings between the proposed technique and the existing methods on CT images.

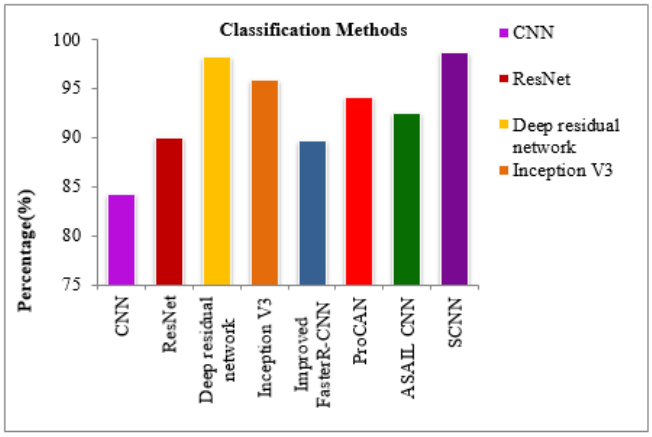

Fig. 6. Comparative analysis of the proposed method and existing methods on CT images.

The comparative analysis of Lung cancer detection in terms of accuracy of the proposed Spiking CNN model with existing methods on Chest X-Ray dataset is displayed in Table V. It is clearly detected that the proposed SCNN classifier gives superior results than the other previous research work based on accuracy. It gives 98.9% of accuracy which is +0.2% than OCNN-SVM approach, +8.8% than Gabor-LBP+MRCNN approach, +25.9% than VDSNet model. The results of this technique's performance comparison with standard methods indicate that the proposed method outperforms them. The intended model yielded better performance than the earlier networks. The expected outcomes seem to be rather reliable in distinguishing between typical and anomalous instances.

Fig. 7 presents a visual representation of the comparison findings between the proposed technique and the existing methods on Chest X-Ray images.

TABLE V. COMPARATIVE ANALYSIS OF SCNN WITH OTHER CLASSIFIERS ON CHEST X-RAY IMAGES

Author/Year	Methods	Accuracy (%)
Bharati et al./2020 [26]	VDSNet	73
Wang et al./2018 [27]	Gabor-LBP+MRCNN	90.1
Sreeprada et al/2023 [28]	OCNN-SVM	98.7
Proposed Method	SCNN	98.9

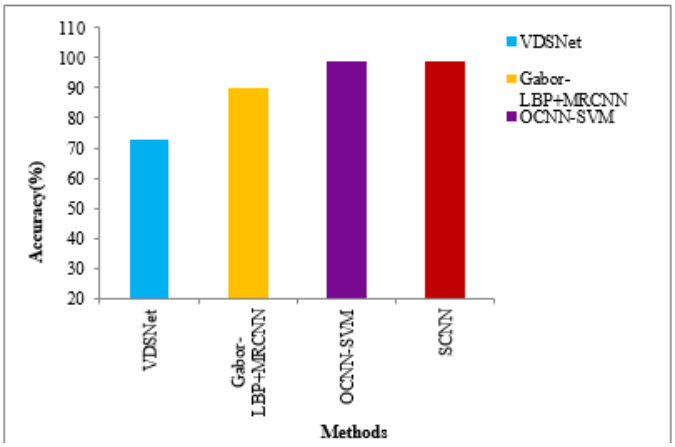

Fig. 7. Comparative analysis of the proposed method and existing methods on Chest X-Ray images.

The pre-processing, segmentation, and classification outcomes of the suggested work are shown in Fig. 8. The original CTX and CT pictures are displayed in the first column. The pre-processing results using CLAHE are shown in the second column. The segmentation result using the Honey Badger method is displayed in the third column. The categorization result is shown by the value in the final column. With the CT image dataset, the suggested operator achieves 98.64% classification accuracy, and with the CXT dataset, it achieves 98.9% accuracy.

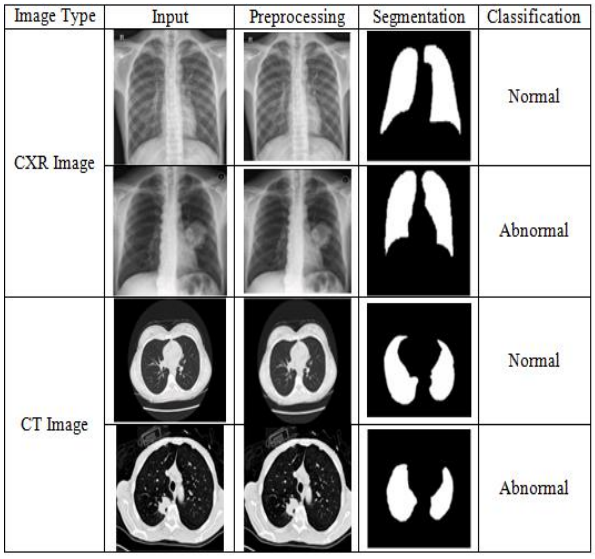

Fig. 8. The segmentation, feature extraction and classification results of proposed work.

VII. DISCUSSION

A very efficient lung image analysis pipeline is a result of the synergy between CLAHE, HBA, and SCNNs. The utilization of contrast enhancement in CLAHE proven to be crucial in emphasizing nuanced traits that are necessary for precise segmentation and classification. Because of its dynamic nature, the Honey Badger Algorithm ensured accurate segmentation even in difficult situations, minimizing errors that could have spread to the classification stage. The excellent accuracy and computational efficiency that SCNNs brought made them a good choice for use in healthcare settings where prompt and dependable decision-making is crucial. The outcomes demonstrate that this integrated strategy, which offers a well-balanced mix of accuracy, efficiency, and interpretability, is well-suited to meet the difficulties associated with lung image processing.

VIII. CONCLUSION

This study proposed a novel neural network model (SCNN) for lung nodule classification, which combines the theories of deep learning, blockchain, and dynamic pattern features to address the issues with lung nodule classification, including a difficult classification detection process and low classification accuracy. The CT scan and CXR image databases from the NIH Chest X-ray and LIDC-IDRI were used. Initially, these images are pre-processed by Contrast Limited Adaptive Histogram Equalization (CLAHE) to enhance the image clarity and reducing the noise. Then the Honey Badger optimization Algorithm (HBA) is used to segment the lung region from the pre-processed image. Morphological segments of the lung region are used to generate dynamic patterns. Finally, these patterns are aggregated into the deep neural Spiking Convolutional Neural Network (SCNN) is the global model for classifying the images into normal and abnormal cases. Based on the LIDC-IDRI and NH Chest X-Ray, the SCNN model achieves 98.64% and 98.9% of accuracy respectively. This methodology provides a comprehensive solution that tackles the particular issues of lung image analysis by combining strong preprocessing, sophisticated segmentation, and effective classification. In the end, the suggested method improves patient outcomes in the field of lung health by laying the groundwork for more precise, understandable, and resource-efficient diagnostic instruments.

REFERENCES

[1] B.U. Dhaware, A.C. Pise, "Lung Cancer Detection Using Bayasein Classifier and FCM Segmentation." IEEE, International Conference on Automatic Control and Dynamic Optimization Techniques (ICACDOT), pp. 170–174, 2016.

[2] American Cancer Society. Cancer Facts and Figures 2022. Atlanta; American Cancer Society: 2022.

[3] K.D. Miller, L. Nogueira, A.B. Mariotto, J.H. Rowland, K.R. Yabroff, C.M. Alfano, R. L. Siegel, "Cancer treatment and survivorship statistics," 2019. CA: A Cancer Journal for Clinicians, 2019. doi:10.3322/caac.21565

[4] S.K. Thakur, D.P. Singh, J. Choudhary, "Lung cancer identification: a review on detection and classification," Cancer Metastasis Rev. vol. 39, pp. 989–998, 2020. https:// doi.org/10.1007/s10555-020-09901-x.

[5] J. Liang, G. Ye, J. Guo, Q. Huang, and S. Zhang, "Reducing False-Positives in Lung Nodules Detection Using Balanced Datasets." Frontiers in public health, vol. 9, pp. 671070, 2021. https://doi.org/10.3389/fpubh.2021.671070

[6] A. Asuntha, A. Srinivasan, "Deep learning for lung Cancer detection and classification." Multimed Tools Appl, vol. 79, pp. 7731–7762, 2020. doi:10.1007/s11042-019-08394-3

[7] M. Vas, and A. Dessai, "Lung cancer detection system using lung CT image processing. 2017 International Conference on Computing, Communication," Control and Automation (ICCUBEA), 2017. doi:10.1109/iccubea.2017.8463851

[8] Y. Li, Q. Wu, H. Sun, and X. Wang, "Research on Lung Nodule Detection Based on Improved Target Detection Network." Complexity, pp. 1–7, 2020. https://doi.org/10.1155/2020/6633242

[9] A. Elnakib, M. Amer, and E.Z. Abou-Chadi, "Early Lung Cancer Detection using Deep Learning Optimization." International Journal of Online and Biomedical Engineering (iJOE), vol. 16, no. 06, pp. 82, 2020. doi:10.3991/ijoe.v16i06.13657.

[10] A. Srinivasulu, K. Ramanjaneyulu, R. Neelaveni, S.R. Karanam, S. Majji, M. Jothilingam, and T.R. Patnala, "Advanced lung cancer prediction based on blockchain material using extended CNN." Applied Nanoscience, 2021. doi:10.1007/s13204-021-01897-2

[11] D. Vaishnavi. K. Arya. Devi Abirami. M.N. Kavitha, "Lung Ancer Detection using Machine Learning", International Journal of Engineering Research & Technology (IJERT), 2019.

[12] Y. Su, D. Li, X. Chen, "Lung nodule detection based on faster R-CNN framework," Comput. Methods Progr. Biomed. vol. 200, pp. 105866, 2021. https://doi.org/10.1016/j.cmpb.2020.105866.

[13] T. Vaiyapuri, Liyakathunisa, H. Alaskar, R., Parvathi, V., Pattabiraman, A. Hussain, "CAT Swarm Optimization-Based ComputerAided Diagnosis Model for Lung Cancer Classification in Computed Tomography Images." Appl. Sci., vol. 12, pp. 5491, 2022.

[14] Rajasekar, Vani and M.P. Vaishnnave, and Sivakumar, Premkumar and Sarveshwaran, Velliangiri and V. Rangaraaj, "Lung cancer disease prediction with CT scan and histopathological images feature analysis using deep learning techniques." Results in Engineering, vol. 18, 2023. 101111. 10.1016/j.rineng.2023.101111.

[15] I.W. Harsono, S. Liawatimena, T.W. Cenggoro," Lung Nodule Detection and Classification from Thorax CT-scan Using RetinaNet with Transfer Learning," Journal of King Saud University-Computer and Information Sciences, 2020, https://doi.org/10.1016/j.jksuci.2020.03.013.

[16] M. Schultheiss, P. Schmette, J. Bodden, et al. "Lung nodule detection in chest X-rays using synthetic ground-truth data comparing CNN-based diagnosis to human performance." Sci Rep, vol. 11, pp. 15857, 2021. https://doi.org/10.1038/s41598-021-94750-z

[17] W. Shen, M. Zhou, F. Yang, Dongdong Yu, Di Dong, Caiyun Yang, Yali Zang, Jie Tian, "Multi-crop Convolutional Neural Networks for lung nodule malignancy suspiciousness classification," Pattern Recognition, vol. 61, pp. 663-673, 2017.doi: 10.1016/j.patcog.2016.05.029.

[18] S. Lal, and M. Chandra, "Efficient algorithm for contrast enhancement of natural images." The International Arab Journal of Information Technology, vol. 11, no. 1, pp. 95–102, 2014.

[19] R. Kumar Rai, P. Gour, and B. Singh, "Underwater image segmentation using CLAHE enhancement and thresholding." International Journal of Emerging Technology and Advanced Engineering, vol. 2, no. 1, pp. 118–123, 2012.

[20] Q. Song, L. Zhao, X. Luo, and X. Dou, "Using deep learning for classification of lung nodules on computed tomography images," Journal of Healthcare Engineering, pp. 7, August 2017.

[21] A. Nibali, Z. He, and D. Wollersheim, "Pulmonary nodule classification with deep residual networks," International Journal of Computer Assisted Radiology and Surgery, vol. 12, pp. 1799–1808, 2017.

[22] P. Wu, X. Sun, Z. Zhao, H. Wang, S. Pan, B. Schuller, "Classification of Lung Nodules Based on Deep Residual Networks and Migration Learning." Comput Intell Neurosci. 2020 Mar 30, pp. 8975078. doi: 10.1155/2020/8975078

[23] L.I. Shiwei, D. Liu, "Automated classification of solitary pulmonary nodules using convolutional neural network based on transfer learning strategy." J. Mech. Med. Biol. Vol. 21, pp. 2140002, 2021.

[24] M. Al-Shabi, K. Shak, M. Tan, “ProCAN: Progressive growing channel attentive non-local network for lung nodule classification.” Pattern Recognit. vol. 122, pp. 108309, 2022.

[25] S. Parveen Banu, M. Syed Mohamed, "Asial CNN: Assorted Scale Integrated Alternate Link Model Convolutional Neural Network for Lung Nodule Detection," *International Journal of Engineering Trends and Technology*, vol. 70, no. 11, pp. 353-363, 2022. Crossref, doi:10.14445/22315381/IJETT-V70I11P237

[26] S. Bharati, P. Podder, and M.R.H. Mondal, “Hybrid deep learning for detecting lung diseases from X-ray images. Informatics in Medicine Unlocked, vol. 20, pp. 100391, 2020. doi:10.1016/j.imu.2020.100391

[27] Q. Wang, Y. Zheng, G. Yang, W. Jin, X. Chen, and Y. Yin, “Multiscale Rotation-Invariant Convolutional Neural Networks for Lung Texture Classification.” IEEE Journal of Biomedical and Health Informatics, vol. 22, no. 1, pp. 184–195, 2018. doi:10.1109/jbhi.2017.2685586

[28] V. Sreeprada, K. Vedavathi, “Lung Cancer Detection from X-Ray Images using Hybrid Deep Learning Technique,” Procedia Computer Science, vol. 230, pp. 467-474, 2023. https://doi.org/10.1016/j.procs.2023.12.102.